

Controllable Band Alignment Transition in InSe–MoS₂ Van der Waals Heterostructure

Xi Chen, Zheng-Zhe Lin,* and Ming Ju

Van der Waals (vdW) heterojunctions with type-II band alignment, in which electrons and holes are localized in distinct layers, play a central role in optoelectronic devices and solar cells. The present study analyzes a type-I→II band alignment transition in InSe–MoS₂ vdW heterostructure, proposed to be controlled via changing interlayer distance or applying perpendicular external electric field. The band position shift of InSe relative to that of MoS₂ attributes to a surface polarization mechanism. Changing band offset into type II facilitates possible use and allows greater flexibility for band engineering of InSe–MoS₂ heterostructure in optoelectronic and solar energy applications. The present findings provide theoretical guidance to a new approach to improve the optoelectronic properties of vdW heterostructures.

The birth of two-dimensional materials launched a great revolution in material science. Several two-dimensional materials have been considered as building blocks for future nanoelectronics and optoelectronics. They can lead to drastic reduction in characteristic lengths of electronic devices.^[1–3] As isolated atomic planes, two-dimensional materials can be reassembled by designing layered heterostructures, which are often called van der Waals (vdW) heterostructures.^[4–6] With distinctive electronic and optoelectronic properties,^[7–11] vdW heterostructures have awakened many research efforts for their potential applications in light-emitting diodes, solar cells, and high-electron-mobility transistors. At present, vdW heterostructures built by graphene,^[12–14] phosphorene,^[15] and transition-metal dichalcogenides (TMDs)^[16–18] have been studied in experiments and theory. A strong photoinduced modulation doping effects in graphene-BN vdW heterostructures were found.^[19] As building blocks, different two-dimensional materials can assemble various vdW heterostructures, revealing new physical properties and phenomena.

Dr. X. Chen, Prof. Z. -Z. Lin
School of Physics and Optoelectronic Engineering
Xidian University
Xi'an 710071, P.R. China
E-mail: zzlin@xidian.edu.cn

Dr. M. Ju
School of Economics and Management
Shanghai Technical Institute of Electronics and Information
Shanghai 200018-201411, P.R. China

 The ORCID identification number(s) for the author(s) of this article can be found under <https://doi.org/10.1002/pssr.201800102>.

DOI: 10.1002/pssr.201800102

The band alignment of vdW heterostructures is crucial in applications of optoelectronics. Several experimental investigations have shown that underlying type-II band alignment is required for optoelectronics and solar cell applications.^[16,20,21] For two-dimensional vdW heterostructures with type-II band alignment, electrons and holes are spatially separated in distinct layers and form interlayer excitons, thus electron-hole recombination could be avoided. Such spatial charge separation leads to long electron-hole recombination lifetime^[22,23] and plays a central role in the internal process of solar cells.^[24] If the band alignment can be controlled and switched to type-II, more vdW heterostructures are

then suitable for optoelectronic and solar energy applications.

In recent years, research efforts have been centered upon devices based on two-dimensional semiconductors such as TMDs and black phosphorene attributed to their exotic properties.^[25–27] Recently, indium selenide (InSe)^[28] which belongs to III-VI layered semiconductor family has been successfully prepared.^[29] On the one hand, Single-layer InSe exhibits high carrier mobility up to $10^3 \text{ cm}^2 \text{ V}^{-1} \text{ s}^{-1}$,^[30,31] high on-off current ratio ($\approx 10^3$), and large broadband spectral response.^[32] Considered as key elements for optoelectronic and nanoelectronic applications attributed to its novel properties, InSe has attracted great interest.^[30,33–36] On the other hand, two-dimensional TMDs have also proved promising fundamental building blocks for ultrathin high-performance devices.^[37–39] Research works have demonstrated and predicted that TMD field-effect transistors show high on/off current ratio ($10^4 \approx 10^8$) with less short-channel effects. Considering InSe–MoS₂ heterostructure has been grown by molecular beam epitaxy,^[40] the band engineering in InSe–MoS₂ vdW heterostructure is worth studying.

The goal of this paper is to investigate the band structure and properties of two-dimensional InSe–MoS₂ vdW heterostructure based on density functional theory (DFT) calculations. The InSe–MoS₂ heterostructure presents a type-I→II band alignment transition, controlled by changing interlayer distance. The band position shift of InSe relative to that of MoS₂ attributes to a surface polarization mechanism. Moreover, it is showed that the type-I→II band alignment transition can be also realized by the application of perpendicular external electric field. This allows manipulation of the band properties and flexibility for band engineering of InSe–MoS₂ heterostructure in optoelectronic and solar energy applications. The present results are essential to the design of future nanoelectronic and optoelectronic devices and

propose a new approach to improve the properties of two-dimensional vdW heterostructures.

Computational Methods: In the simulation model, 3×3 InSe monolayer is matched to 4×4 MoS₂ monolayer. The lattice constant mismatch is less than 2%. Periodic boundary conditions are applied. To avoid the interactions between nearest slabs, the replicas of simulation systems are separated by a large spacing of 30 Å along the z direction (perpendicular to the two-dimensional surface).

First-principles calculations are performed within spin-polarized DFT by using Vienna ab initio simulation package (VASP).^[41] Projector-augmented wave (PAW) method^[42] is used to account electron-ion interactions. In all the calculations, a plane-wave basis set with kinetic energy cutoff of 400 eV is used to expand the wave functions. The convergence of the total energy was considered to be achieved until two iterated steps with energy difference less than 10^{-5} eV. The Brillouin zone is sampled by using $3 \times 3 \times 1$ Γ -centered Monkhorst–Pack grid. A Gaussian smearing with a width of $\sigma = 0.05$ eV is used.

In geometry optimizations and total energy calculations, the optB88-vdW dispersion-corrected exchange functional,^[43,44] which has been demonstrated as a reliable approach to describe dispersive forces in 2D systems,^[45] is employed to correctly describe the effect of a vdW interaction. Geometry optimizations are performed until the Hellmann–Feynman forces acting on each atom are less than 0.01 eV \AA^{-1} . Ground state structures are found by using the conjugate gradient method.

To account for the band gaps and band edge positions, the Heyd–Scuseria–Ernzerhof (HSE06) hybrid functional^[46,47] is used to calculate the band structures of the optimized systems. In general, HSE06 hybrid functional provides more accurate band gaps as well as band alignment. The band structures and absolute band energies are aligned with respect to the vacuum level obtained via electrostatic potential.

Basic properties and band alignment: The InSe monolayer lattice (Figure 1a) has hexagonal symmetry, with a thickness of four atoms linked in the Se–In–In–Se sequence via covalent

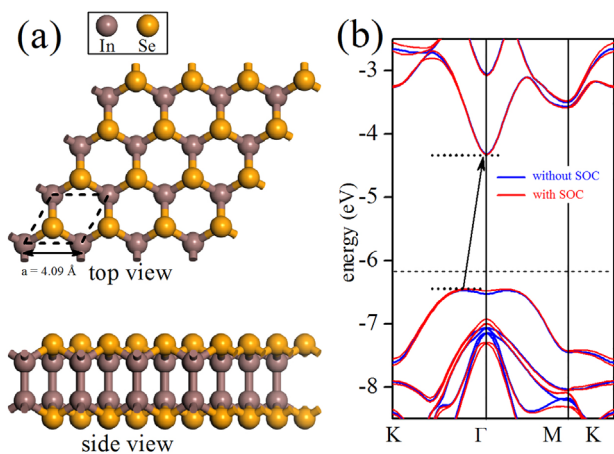


Figure 1. Basic properties of InSe monolayer. a) Top and side view of InSe monolayer. b) Band structure of InSe monolayer at the level of HSE06. Red and blue lines denote the calculation results with and without SOC, respectively. The Fermi level is shown by dashed line. The energy of vacuum level is set zero.

bonds with the In atoms at tetrahedral sites. The rhombic unit cell is shown by dashed lines in Figure 1a. The calculated lattice constant $a = 4.09 \text{ \AA}$ is in agreement with previous experimental^[28,48] and theoretical^[28,49,50] results. In InSe monolayer, an indirect band gap (shown by the arrow in Figure 1b) is observed, with the conduction band minimum (CBM) at the Γ point and the valence band maximum (VBM) lying between the Γ and K points. The spin-orbit coupling (SOC) induces a splitting of some bands (see red lines in Figure 1b by about 0.1 eV (as seen, e.g., at K, Γ , and M points)). Generally, hybrid HSE06 functional provides more accurate band gap than standard DFT approach. Ideally, one should also employ GW many-body theory to obtain reliable band energies. (It is worth noting that the vertex correction, which is ignored by the GW method, is very important for the band alignment. Recent report indicates that the vertex mainly shifts the bands of two-dimensional semiconductors relative to vacuum by 0.5 eV.^[51]) Here, the Perdew–Burk–Ernzerhof (PBE) functional, HSE06 functional and GW0 calculations (starting from HSE06 orbitals) are performed for InSe single cells to obtain band gap. With the PBE functional, the calculated band gap is 1.42 (1.39) eV with (without) SOC, respectively. With the HSE06 functional, the calculated band gap is 2.15 (2.12) eV with (without) SOC, respectively. The GW0 calculation further increases the band gap. With GW0 calculation, the calculated band gap is 2.96 (2.93) eV with (without) SOC, respectively (in agreement with Debbichi et al.^[28]). The differences between PBE, HSE06 and GW0 calculations are mostly a shift of band structure. The GW0 calculation provides more accurate band gap, but takes much more computation time. So, in the following text, HSE06 functional is employed without SOC for all the calculations.

Before investigating the properties of InSe–MoS₂ heterostructure, we first understand the band alignment of InSe and MoS₂ monolayers. DFT calculations suggest a band alignment transition in the combination of InSe and MoS₂ monolayers. For isolated InSe and MoS₂ monolayers, the band structures are predicted to be type-II band alignment (Figure 2a), i.e., the VBM of MoS₂ is higher than the VBM of InSe ($\Delta_{\text{VB}} = E_{\text{MoS}_2}^{\text{VBM}} - E_{\text{InSe}}^{\text{VBM}} > 0$), and meanwhile, the CBM of MoS₂ is higher than the CBM of InSe ($\Delta_{\text{CB}} = E_{\text{MoS}_2}^{\text{CBM}} - E_{\text{InSe}}^{\text{CBM}} > 0$). When the InSe and MoS₂

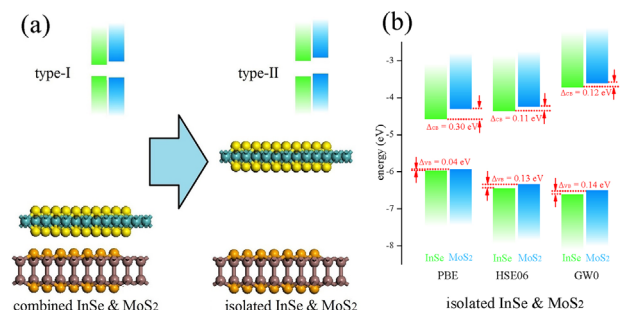


Figure 2. Band alignment of InSe and MoS₂. a) Isolated and combined InSe and MoS₂ monolayers. b) Calculated band alignment of separated InSe and MoS₂ monolayers at the level of PBE, HSE06 and GW0. The energy of vacuum level is set zero.

monolayers constitute vdW heterostructure, the band alignment changes into type-I (Figure 2a), i.e., $\Delta_{VB} = E_{\text{MoS}_2}^{\text{VBM}} - E_{\text{InSe}}^{\text{VBM}} < 0$ and $\Delta_{CB} = E_{\text{MoS}_2}^{\text{CBM}} - E_{\text{InSe}}^{\text{CBM}} > 0$. To verify the reliability of our calculations, the band structures of isolated InSe and MoS₂ monolayers are calculated by using PBE, HSE06 and GW0 calculations (Figure 2b). The PBE calculation provides band offset $\Delta_{VB} = E_{\text{MoS}_2}^{\text{VBM}} - E_{\text{InSe}}^{\text{VBM}} = 0.04$ eV and $\Delta_{CB} = E_{\text{MoS}_2}^{\text{CBM}} - E_{\text{InSe}}^{\text{CBM}} = 0.03$ eV. However, the PBE result may be quantitatively inaccurate, while the HSE06 and GW0 results are more reliable.

The HSE06 calculation provides $\Delta_{VB} = 0.13$ eV and $\Delta_{CB} = 0.11$ eV. The GW0 calculation provides larger band gaps than HSE06, and the GW0-predicted band offset $\Delta_{VB} = 0.14$ eV and $\Delta_{CB} = 0.12$ eV are similar to HSE06. Although HSE06 still underestimates the band gaps relative to GW0 by 0.81 eV for InSe and 0.81 eV for MoS₂, the HSE06 is significantly closer to the GW0 result than the PBE. Therefore, HSE06 functional is used throughout the paper for band offset calculations.

Band alignment control via interlayer distance control: In this section, we study controlling the band alignment of InSe–MoS₂

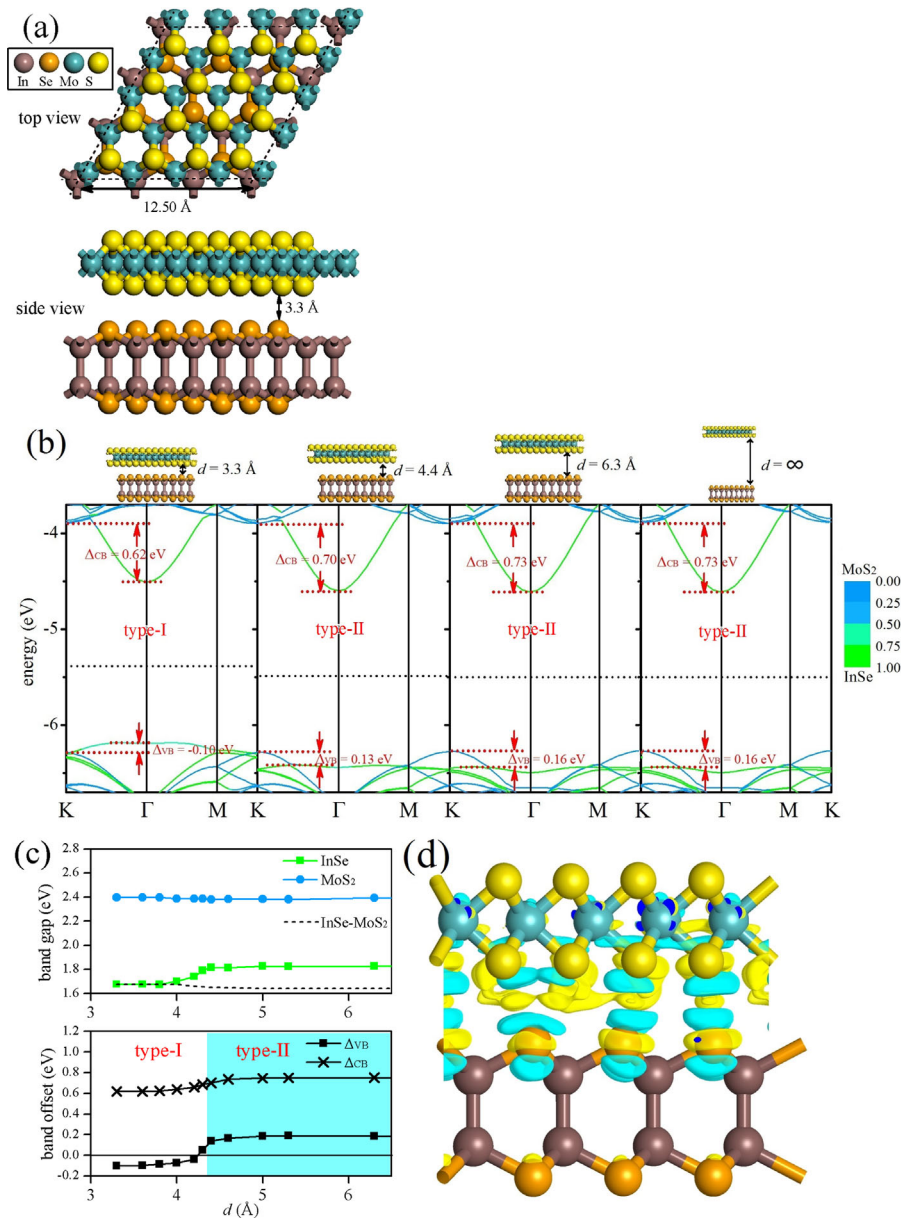


Figure 3. The band structure and alignment of InSe–MoS₂ heterojunction changing with interlayer distance. a) The top and side views of InSe–MoS₂ vdW heterostructure. Periodic boundary is shown by dashed lines. b) Projected band structure of InSe–MoS₂ heterostructure at the level of HSE06 with interlayer distance $d = 3.3, 4.3, 6.3,$ and ∞ Å. The green projection comes from the InSe layer and the blue comes from the MoS₂ layer. The Fermi level is shown by dashed lines. The energy of vacuum level is set zero. c) The band gap (upper) and band offset (lower) varying with enlarging InSe–MoS₂ distance d . d) Isosurfaces of charge redistribution with values of $\pm 10^{-4} \text{ e} \text{ \AA}^{-3}$ (cyan/yellow respectively) for $d = 3.3$ Å.

heterostructure via changing the interlayer distance. The simulation model of InSe–MoS₂ vdW heterostructure is set up by matching 3 × 3 InSe monolayer to 4 × 4 MoS₂ monolayer (Figure 3a), with a supercell lattice constant of 12.50 Å. The lattice constant mismatch of InSe (MoS₂) is +1.8 (−1.9)%, respectively. In the most stable structure, the vertical distance from the bottom of MoS₂ layer to the top of InSe layer is 3.3 Å (Figure 3a). Such distance is larger than the sum of the covalent radii of S and Se atoms, indicating no chemical bonds at the InSe–MoS₂ interface.

Before studying the effect of interlayer distance, we first investigate band properties of the most stable structure of InSe–MoS₂ heterostructure. The 1st of Figure 3b plots the projected band structure of the most stable InSe–MoS₂ heterostructure, with interlayer distance $d = 3.3$ Å. The green projection comes from the InSe layer and the blue comes from the MoS₂ layer. The electronic states of the InSe and the MoS₂ layers are weakly perturbed upon the formation of InSe–MoS₂ heterostructure. We found that the band gap of InSe/MoS₂ change by less than 0.13/0.01 eV, respectively. In the 1st panel of Figure 3b, the InSe–MoS₂ heterostructure presents a type-I band alignment with a valence band offset $\Delta_{VB} = E_{MoS_2}^{VBM} - E_{InSe}^{VBM} = -0.10$ eV and a conduction band offset $\Delta_{CB} = E_{MoS_2}^{CBM} - E_{InSe}^{CBM} = 0.62$ eV.

Next, we gradually enlarge the interlayer distance d and observe the change of band structure. The lower panel of Figure 3c plots Δ_{VB} and Δ_{CB} varying with enlarging InSe–MoS₂ distance d . In the range of $d = 4 \approx 5$ Å, the band alignment of InSe–MoS₂ heterostructure changes from type-I ($\Delta_{VB} < 0$ and $\Delta_{CB} > 0$) to type-II ($\Delta_{VB} > 0$ and $\Delta_{CB} > 0$). In the 2nd panel of Figure 3b, the band structure of InSe–MoS₂ heterostructure with $d = 4.4$ Å is depicted, presenting a type-II band alignment with $\Delta_{VB} = 0.13$ eV and $\Delta_{CB} = 0.70$ eV. The InSe–MoS₂ heterostructure presents a semiconducting character with an indirect band gap of 1.68 eV, with VBM at the K point and CBM lying at the Γ point. In the projected band structure of Figure 3b, we can see that VBM lies on the InSe layer while CBM is localized in the MoS₂ layer, which is suitable in order to promote the electron-hole separation. With enlarging interlayer distance $d > 4.4$ Å, the band structure of InSe–MoS₂ heterostructure only has a little change. The 3rd panel of Figure 3b depicts the band structure of $d = 6.3$ Å, presenting a type-II band alignment with $\Delta_{VB} = 0.16$ eV and $\Delta_{CB} = 0.73$ eV which are almost equivalent to those of isolated InSe and MoS₂ layers (the 4th panel of Figure 3b).

In terms of change of interlayer distance d , the band gap slightly changes with it. The upper panel of Figure 3c plots the band gap of InSe and MoS₂, and the band gap of InSe–MoS₂ heterostructure. In the range of $d = 3.3 \approx 9.3$ Å, the band gap of MoS₂ seldom changes, while the band gap of InSe slightly increases. In the change of d , the band gap of InSe–MoS₂ heterostructure changes a little, from 1.68 to 1.66 eV. According to results above, the change of interlayer distance d only affects band alignment of InSe–MoS₂ heterostructure but seldom changes band gap. This characteristic is beneficial for the use of InSe–MoS₂ heterostructure as adjustable device, with flexible control of band alignment and without changing band gap.

To gain more insight into the change of band alignment, we pay attention to the interaction and charge redistribution between InSe and MoS₂ layers. As the InSe and MoS₂ layers have different Fermi

energy, electrons would slightly redistribute when the two layers get close to each other, leading to the rise/drop of InSe/MoS₂ valence band. To visualize the charge redistribution, we plot the isosurface of charge redistribution in the InSe–MoS₂ heterostructure for the case of $d = 3.3$ Å in Figure 3d. It can be seen that slight charge redistribution happens mainly in the region between the InSe and MoS₂ layers. In the InSe layer, the electrons are repulsed by the MoS₂ layer, showing more negative charge area near the centers of Se atoms. Such repulsion leads to the enhancement of InSe valence band. On the contrary, in the MoS₂ layer the electrons are attracted by the InSe layer, showing more negative charge area in the region between the InSe and MoS₂ layers. Such electronic attraction on MoS₂ leads to the reduction of MoS₂ valence band. The electron redistribution reveals a polarization near InSe–MoS₂ contact surface that causes the slight interaction between InSe and MoS₂ layers.

In addition, the stability of InSe–MoS₂ heterostructure is examined by comparing the total energies of relaxed InSe–MoS₂ system ($U_{InSe-MoS_2}$) with ones of isolated InSe and MoS₂ layers (U_{InSe} and U_{MoS_2}). The U_{InSe} and U_{MoS_2} are obtained by considering the strained 3 × 3 InSe and 4 × 4 MoS₂ supercells. The binding potential is calculated as $U^b = U_{InSe-MoS_2} - (U_{InSe} + U_{MoS_2}) = -18.9$ meV Å^{−2}, which is lower than the binding potential of InSe-phosphorene heterostructure (−9.03 meV Å^{−2}).^[36] The stability of InSe–MoS₂ heterostructure is further revealed by the change of interlayer binding energy. Starting from interlayer balance distance $d = 3.3$ Å, interlayer binding energy U^b decreases with enlarging d (Figure 4). In the range of $d = 3.3 \approx 5.0$ Å, $U^b = -18.9 \approx -8.93$ meV Å^{−2} keeps lower than the binding potential of InSe-phosphorene heterostructure. In this range of d , InSe–MoS₂ heterostructure keeps more stable than InSe-phosphorene heterostructure. When manipulating the band alignment via changing interlayer

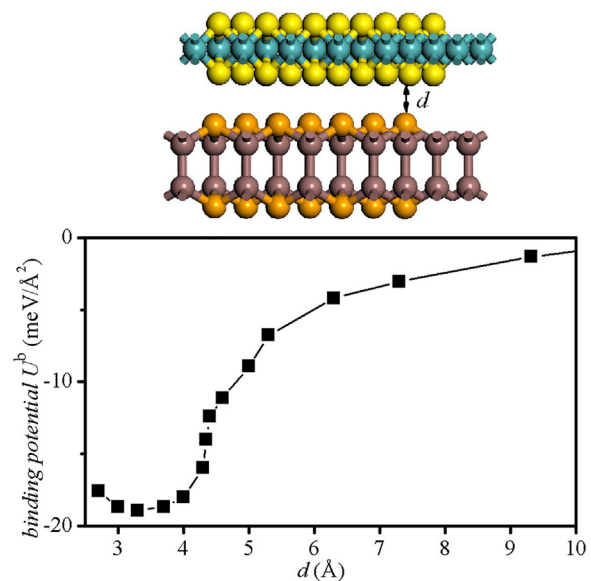


Figure 4. Energetics of InSe–MoS₂ heterostructure. The change of InSe–MoS₂ binding energy U^b with interlayer distance d .

distance in this range, the stability of InSe–MoS₂ heterostructure could be guaranteed.

Band alignment control via external electric field: In this section, we further consider controlling the the band alignment via applying external electric field. For InSe–MoS₂ heterostructure in the equilibrium interlayer distance $d = 3.3 \text{ \AA}$ (type-I band alignment, $\Delta_{\text{VB}} = E_{\text{MoS}_2}^{\text{VBM}} - E_{\text{InSe}}^{\text{VBM}} < 0$), an external electric field pointing from MoS₂ to InSe is applied. Then, electrons drift from InSe to MoS₂ and the band alignment would change from type-I to type-II. **Figure 5a** plots the projected band structure with perpendicular external field $\varepsilon = 0, 0.2, \text{ and } 0.4 \text{ eV \AA}^{-1}$. It can be seen that the band of InSe gradually moves down relative to that of MoS₂ with increasing electric field, leading to enlarging Δ_{VB} and Δ_{CB} . For $\varepsilon > 0.2 \text{ eV \AA}^{-1}$, the band alignment is changed o type-II ($\Delta_{\text{VB}} = E_{\text{MoS}_2}^{\text{VBM}} - E_{\text{InSe}}^{\text{VBM}} < 0$). The lower panel of **Figure 5b** plots the change of Δ_{VB} and Δ_{CB} along with external electric field $\varepsilon = -0.2 \approx 0.4 \text{ eV \AA}^{-1}$. The result above offers us a simple way to control the band alignment by applying bias voltage on the InSe–MoS₂ heterostructure. For $d = 3.3 \text{ \AA}$, a voltage of $0 \approx 2 \text{ V}$ can generate an electric field of about $0 \approx 0.6 \text{ V \AA}^{-1}$, which is large enough for the band offset control. We then perform detailed calculations for external field $\varepsilon = -0.2 \approx 0.4 \text{ eV \AA}^{-1}$, and find linear relation of band gap dependent on ε (**Figure 5b**).

Conclusion: In conclusion, the InSe–MoS₂ heterostructure possesses well-controlled interfacial electronic properties and band structure which could be manipulated by changing

interlayer distance or applying external electric field. DFT calculations reveal the stability of two-dimensional InSe–MoS₂ vdW heterostructure. It is evident that there are no chemical bonds at the InSe–MoS₂ interface. The electronic states of InSe and MoS₂ layers are mostly preserved upon the formation of InSe–MoS₂ heterostructure, and nearly independent of parallel displacement of MoS₂ on InSe. An intrinsic change from type-I to type II band alignment occurs with enlarging interlayer distance. The shift of the band position of InSe relative to that of MoS₂ attributes to a surface polarization mechanism, leading to slight electron redistribution between the InSe and MoS₂ layers. Moreover, it is also possible to invoke the type-I→II band alignment transition by applying perpendicular external electric field or bias voltage. Overall, changing band offset to type II leads to possible use of InSe–MoS₂ heterostructure in optoelectronic and solar energy applications. Our research proposes a new perspective on advantage nanoelectronic and optoelectronic devices with well-controlled feature of vdW heterostructures, and also provides theoretical guidance on improving the optoelectronic properties of vdW heterostructures.

Acknowledgements

This work was financially supported by the Fundamental Research Funds for the Central Universities (No. JB180513) and the 111 Project (No. B17035).

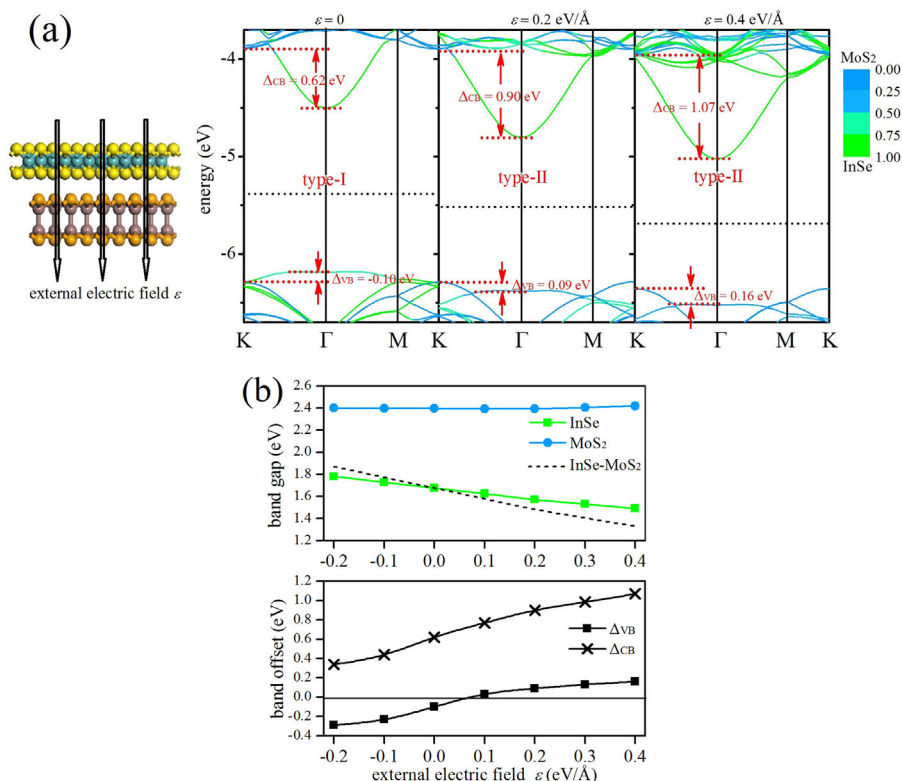


Figure 5. The band structure and alignment of InSe–MoS₂ heterojunction changing with external electric field. a) Projected band structure of InSe–MoS₂ heterostructure at the level of HSE06 with interlayer distance $d = 3.3 \text{ \AA}$, and perpendicular external field $\varepsilon = 0, 0.2 \text{ and } 0.4 \text{ eV \AA}^{-1}$. The Fermi level is shown by dashed line. b) The band gap (upper) and band offset (lower) varying with external electric field.

Conflict of Interest

The authors declare no conflict of interest.

Keywords

controllable band alignment, type-I→II transition, two-dimensional van der Waals heterojunctions

Received: March 6, 2018

Revised: April 8, 2018

Published online: April 18, 2018

- [1] S. Z. Butler, S. M. Hollen, L. Cao, Y. Cui, J. A. Gupta, H. R. Gutierrez, T. F. Heinz, S. S. Hong, J. Huang, A. F. Ismach, E. Johnston-Halperin, M. Kuno, V. V. Plashnitsa, R. D. Robinson, R. S. Ruoff, S. Salahuddin, J. Shan, L. Shi, M. G. Spencer, M. Terrones, W. Windl, J. E. Goldberger, *ACS Nano* **2013**, *7*, 2898.
- [2] J. M. Hamm, O. Hess, *Science* **2013**, *340*, 1298.
- [3] K. J. Koski, Y. Cui, *ACS Nano* **2013**, *7*, 3739.
- [4] L. Britnell, R. V. Gorbachev, R. Jalil, B. D. Belle, F. Schedin, A. Mishchenko, T. Georgiou, M. I. Katsnelson, L. Eaves, S. V. Morozov, N. M. R. Peres, J. Leist, A. K. Geim, K. S. Novoselov, L. A. Ponomarenko, *Science* **2012**, *335*, 947.
- [5] A. K. Geim, I. V. Grigorieva, *Nature* **2013**, *499*, 419.
- [6] R. Balu, X. L. Zhong, R. Pandey, S. P. Karna, *Appl. Phys. Lett.* **2012**, *100*, 1530.
- [7] H.-P. Komsa, A. V. Krasheninnikov, *Phys. Rev. B* **2013**, *88*, 085318.
- [8] W. Li, T. Wang, X. Dai, X. Wang, C. Zhai, Y. Ma, S. Chang, *Solid State Commun.* **2016**, *225*, 32.
- [9] X. Liu, Z. Li, *J. Phys. Chem. Lett.* **2015**, *6*, 3269.
- [10] A. Ramasubramaniam, D. Naveh, E. Towe, *Phys. Rev. B* **2011**, *84*, 3239.
- [11] C. Tan, Q. Yang, R. Meng, Q. Liang, J. Jiang, X. Sun, H. Ye, X. P. Chen, *J. Mat. Chem. C* **2016**, *4*, 8171.
- [12] W. Li, T.-X. Wang, X.-Q. Dai, X.-L. Wang, Y.-Q. Ma, S.-S. Chang, Y.-N. Tang, *Physica E* **2017**, *88*, 6.
- [13] J. E. Padilha, A. Fazzio, A. J. R. da Silva, *Phys. Rev. Lett.* **2015**, *114*, 066803.
- [14] F. Zhang, W. Li, X. Dai, *Superlattices Microstruct.* **2016**, *100*, 826.
- [15] L. Huang, J. Li, *Appl. Phys. Lett.* **2016**, *108*, 147.
- [16] H. Fang, C. Battaglia, C. Carraro, S. Nemsak, B. Ozdol, J. S. Kang, H. A. Bechtel, S. B. Desai, F. Kronast, A. A. Unal, G. Conti, C. Conlon, G. K. Palsson, M. C. Martin, A. M. Minor, C. S. Fadley, E. Yablonovitch, R. Maboudian, A. Javey, *Proc. Natl. Acad. Sci. USA* **2014**, *111*, 6198.
- [17] Y. Ma, X. Zhao, T. Wang, W. Li, X. Wang, S. Chang, Y. Li, M. Zhao, X. Dai, *Phys. Chem. Chem. Phys.* **2016**, *18*, 28466.
- [18] S. Latini, K. T. Winther, T. Olsen, K. S. Thygesen, *Nano Lett.* **2017**, *17*, 938.
- [19] L. Jun, J. Velasco, Jr., E. Huang, S. Kahn, C. Nosiola, H.-Z. Tsai, W. Yang, T. Taniguchi, K. Watanabe, Y. Zhang, G. Zhang, M. Crommie, A. Zettl, F. Wang, *Nature Nanotechnol.* **2014**, *9*, 348.
- [20] H. Heo, J. H. Sung, S. Cha, B.-G. Jang, J.-Y. Kim, G. Jin, D. Lee, J.-H. Ahn, M.-J. Lee, J. H. Shim, H. Choi, M.-H. Jo, *Nature Commun.* **2015**, *6*, 7372.
- [21] P. Rivera, K. L. Seyler, H. Yu, J. R. Schaibley, J. Yan, D. G. Mandrus, W. Yao, X. Xu, *Science* **2016**, *351*, 688.
- [22] M. Palummo, M. Bernardi, J. C. Grossman, *Nano Lett.* **2015**, *15*, 2794.
- [23] P. Rivera, J. R. Schaibley, A. M. Jones, J. S. Ross, S. Wu, G. Aivazian, P. Klement, K. Seyler, G. Clark, N. J. Ghimire, J. Yan, D. G. Mandrus, W. Yao, X. Xu, *Nature Commun.* **2015**, *6*, 6242.
- [24] C.-H. Lee, G.-H. Lee, A. M. van der Zande, W. Chen, Y. Li, M. Han, X. Cui, G. Arefe, C. Nuckolls, T. F. Heinz, J. Guo, J. Hone, P. Kim, *Nature Nanotechnol.* **2014**, *9*, 676.
- [25] Q. H. Wang, K. Kalantarzadeh, A. Kis, J. N. Coleman, M. S. Strano, *Nature Nanotechnol.* **2012**, *7*, 699.
- [26] R. R. Q. Freitas, R. Rivelino, F. D. B. Mota, C. M. C. D. Castilho, A. Kakanakova-Georgieva, G. K. Gueorguiev, *J. Phys. Chem. C* **2016**, *119*, 23599.
- [27] R. R. Freitas, B. M. F. De, R. Rivelino, C. M. de Castilho, A. Kakanakova-Georgieva, G. K. Gueorguiev, *Nanotechnology* **2016**, *27*, 055704.
- [28] L. Debbichi, O. Eriksson, S. Lebègue, *J. Phys. Chem. Lett.* **2015**, *6*, 3098.
- [29] D. A. Bandurin, A. V. Tyurnina, G. L. Yu, A. Mishchenko, V. Zólyomi, S. V. Morozov, R. K. Kumar, R. V. Gorbachev, Z. R. Kudrynskiy, S. Pezzini, *Nature Nanotechnol.* **2017**, *12*, 223.
- [30] S. Sucharitakul, N. J. Goble, U. R. Kumar, R. Sankar, Z. A. Bogorad, F. C. Chou, Y. T. Chen, X. P. A. Gao, *Nano Lett.* **2015**, *15*, 3815.
- [31] W. Feng, W. Zheng, W. Cao, P. A. Hu, *Adv. Mater.* **2014**, *26*, 6587.
- [32] S. R. Tamalampudi, Y. Y. Lu, U. R. Kumar, R. Sankar, C. D. Liao, B. K. Moorthy, C. H. Cheng, F. C. Chou, Y. T. Chen, *Nano Lett.* **2014**, *14*, 2800.
- [33] S. Lei, F. Wen, L. Ge, S. Najmaei, A. George, Y. Gong, W. Gao, Z. Jin, B. Li, J. Lou, *Nano Lett.* **2015**, *15*, 3048.
- [34] W. Feng, W. Zheng, X. S. Chen, G. Liu, P. A. Hu, *ACS Appl. Mater. Interfaces* **2015**, *7*, 26691.
- [35] H. Jin, J. Li, L. Wan, Y. Dai, Y. Wei, H. Guo, *2D Mater.* **2017**, *4*, 025116.
- [36] J. E. Padilha, R. H. Miwa, A. J. R. D. Silva, A. Fazzio, *Phys. Rev. B* **2017**, *95*, 195143.
- [37] O. Lopez Sanchez, D. Lembke, M. Kayci, A. Radenovic, A. Kis, *Nature Nanotechnol.* **2013**, *8*, 497.
- [38] M. Massicotte, P. Schmidt, F. Violla, K. G. Schädler, A. Reserbatplantey, K. Watanabe, T. Taniguchi, K. J. Tielrooij, F. H. L. Koppens, *Nature Nanotechnol.* **2016**, *11*, 42.
- [39] A. Steinhoff, J. H. Kim, F. Jahnke, M. Rösner, D. S. Kim, C. Lee, G. H. Han, M. S. Jeong, T. O. Wehling, C. Gies, *Nano Lett.* **2015**, *15*, 6841.
- [40] T. Hayashi, K. Ueno, K. Saiki, A. Koma, *J. Cryst. Growth* **2000**, *219*, 115.
- [41] G. Kresse, J. Hafner, *Phys. Rev. B* **1993**, *48*, 13115.
- [42] P. E. Blöchl, *Phys. Rev. B* **1994**, *50*, 17953.
- [43] J. Klimeš, D. R. Bowler, A. Michaelides, *J. Phys.: Condens. Matter* **2010**, *22*, 022201.
- [44] J. Klimeš, D. R. Bowler, A. Michaelides, *Phys. Rev. B* **2011**, *83*, 772.
- [45] H. Y. Guo, N. Lu, J. Dai, X. J. Wu, X. C. Zeng, *J. Phys. Chem. C* **2014**, *118*, 14051.
- [46] J. Heyd, G. E. Scuseria, M. Ernzerhof, *J. Chem. Phys.* **2003**, *118*, 8207.
- [47] J. Heyd, G. E. Scuseria, M. Ernzerhof, *J. Chem. Phys.* **2006**, *124*, 219906.
- [48] A. Politano, D. Campi, M. Cattelan, I. Ben Amara, S. Jaziri, A. Mazzotti, A. Barinov, B. Gurbulak, S. Duman, S. Agnoli, L. S. Caputi, G. Granozzi, A. Cupolillo, *Sci. Rep.* **2017**, *7*, 3445.
- [49] H. Jin, J. W. Li, Y. Dai, Y. D. Wei, *Phys. Chem. Chem. Phys.* **2017**, *19*, 4855.
- [50] H. Jin, J. W. Li, L. H. Wan, Y. Dai, Y. D. Wei, H. Guo, *2D Mater.* **2017**, *4*, 025116.
- [51] P. S. Schmidt, C. E. Patrick, K. S. Thygesen, *Phys. Rev. B* **2017**, *96*, 205206.